Rock and Soil Mechanics

Volume 44 | Issue 1 Article 5

3-13-2023

Experimental study on the mechanism of gas accumulation and soil deformation in double-layered soils

Kai-feng GUO

Yi-ping ZHANG
zhangyiping@zju.edu.cn

Custom Citation

GUO Kai-feng, ZHANG Yi-ping. Experimental study on the mechanism of gas accumulation and soil deformation in double-layered soils[J]. Rock and Soil Mechanics, 2023, 44(1): 99-108.

Rock and Soil Mechanics 2023 44(1): 99−108 ISSN 1000−7598
https: //doi.org/10.16285/j.rsm.2022.5268 rocksoilmech.researchcommons.org/journal

Experimental study on the mechanism of gas accumulation and soil deformation in double-layered soils

GUO Kai-feng, ZHANG Yi-ping

College of Civil Engineering and Architecture, Zhejiang University, Zhejiang, Hangzhou 310058, China

Abstract: Magnesium lithium phyllosilicate (MLPS) transparent soil is used to build a double-layered soil model with upper hard layer and lower soft layer. The gas source generated in the sedimentary layer is simulated by pinhole gas injection. Based on the image recognition technology, the experimental research on the morphology change of gas bubble and the uplift deformation of the upper soil in the process of gas accumulation in the formation is carried out. The results show that: (1) The gas presents different shapes in the process of gas bubble accumulation, and the time and morphology of the gas bubble breakthrough depend on the strength and height of the upper soil. (2) The changes of gas bubble morphology, volume and pressure can be roughly divided into two stages. At the first stage, the gas bubble volume and width increase linearly, while the gas bubble height decreases gradually due to the contraction of the bottom, and the gas pressure increases slowly. At the second stage, the increase of gas bubble width is slowed down, the expansion speed of gas bubble volume is accelerated, the height of gas bubble begins to increase significantly, and the gas bubble pressure decreases rapidly from the highest point. The uplift height and width of the upper soil increase significantly at the second stage. (3) The width and volume of the gas bubble before breakthrough and the uplift width and height of the upper soil have a good fitting relationship with the yield strength and the height of upper transparent soil. (4) The thin plate theory can reasonably explain the mechanism of upper soil deformation caused by gas accumulation, while the medium-to-thick plate theory is not applicable.

Keywords: double-layered soils; magnesium lithium phyllosilicate (MLPS) transparent soil; gas injection test; gas accumulation and breakthrough; soil deformation

1 Introduction

Pore gas can be naturally generated in the soils, and then grows and coalesces into small gas bubbles. They can break surrounding soils and migrate upwards along the induced fractures. The upward migration of small gas bubbles will stop when a harder soil layer is encountered. The small gas bubbles continue to accumulate to form larger gas bubbles, which migrate upwards and eventually break through the soils and are released into the atmosphere[1]. The migration, accumulation and breakthrough phenomena of gases are widely observed in the porous media such as sedimentary layers and landfills in engineering construction, environmental protection, climate change and other fields. During engineering construction and underground space development, underground gas with shallow burial depth and high pressure is frequently released, which brings about numerous engineering problems such as foundation failure, differential settlement and loss of pile bearing capacity[2]. For example, a large amount of gas in the shallow sedimentary layer of Hangzhou Bay causes ground settlement, and gas eruption is also a potential risk to the construction operations[3]. Some of the shallow gas or landfill gas can even cause explosions and fires after accumulating in and breaking through the soils due to the high concentration of methane contained[4]. For another example, the release of greenhouse gases from underwater shallow sediments, such as soft seabed soils and lake sediments, is closely related to global warming[5]. The accumulation, migration and release of gases from submerged shallow sediments can cause changes in sediment structure, thereby increasing the release flux of gases[6]. Therefore, it is of great significance to fully understand the evolution of gas accumulation in soil layer and deformation mechanism of soils to enhance the safety of engineering construction and help environmental and climate management.

Plenty of studies have been carried out on the growth, migration, breakthrough and release of gases in the sediments[7−10]. There are two main modes of gas growth and migration in the sediments: firstly, gas invades into sediment pores through capillaries under capillary pressure (the difference between gas pressure and water pressure), i.e. capillary-controlled invasion[7]; secondly, gas pressure overcomes the compressive stress and friction at the contact of sediment particles, preferentially displacing the particles to initiate a

Received: 28 March 2022 Accepted: 24 May 2022
This work was supported by the National Natural Science Foundation of China (51579219).
First author: GUO Kai-feng, male, born in 1997, Postgraduate, focusing on accumulation and breakthrough mechanisms of gas in sedimentary layers. E-mail: 21912135@zju.edu.cn
Corresponding author: ZHANG Yi-ping, male, born in 1973, PhD, Professor, research interests: soft soil ground and municipal foundation engineering. E-mail: zhangyiping@zju.edu.cn

fracture along which the gas grows, i.e. fracture-dominated invasion[8], and the fracture advances normal to the minimum effective stress direction[9]. Gas growth and accumulation in the sediment are usually followed by breakthrough and release in the way of forming fractures in the overlying layer, i.e. the sediment is destroyed when the gas pressure reaches a certain threshold. The failure modes of sediment include cavity expansion, tensile failure, shear failure, linear elastic fracture, etc. Different failure modes correspond to different theoretical or empirical equations. The critical pressure of gas breakthrough in the sediments is influenced by many factors such as initial stress, strength, stiffness, consolidation conditions and local non-homogeneity of the sediment[10].

In actual geological surveys, several scholars have detected the location, morphology and size of shallow gas accumulation in the Sea of Japan[11], the Mediterranean Sea[12] and the Sea of Okhotsk[13] through acoustic imaging methods. It has been found that the shallow gas stored in the seabed is mainly in layered morphology, and its horizontal dimension is much larger than the thickness of the shallow gas and the height of the overlying layer. In addition, the seabed shallow gas can also exist in forms of gas blocks, high-pressure gas bubbles, and gas diapir after accumulation and migration[14]. Li et al.[15] summarized the distribution, burial depth and area of the shallow gas in China's offshore waters according to the results of land resources survey and analyzed the origin, morphology and hazards of the shallow gas. Tao et al.[16] surveyed the shallow gas under the marine sedimentary soils in Ningbo area by using improved cone penetration testing (CPT) system and detected the composition, burial depth, pressure and flux of the shallow gas, where the gas pressure ranged from 0.015 MPa to 0.200 MPa, and the gas flow ranged from 0.004 m^3 to 0.804 m^3.

Although the early process of gas growth in sediment pores, such as gas bubble nucleation and gas migration mechanism at the microscopic level, has been studied extensively, there is still a lack of in-depth understanding of the subsequent evolution of larger-size gas bubbles accumulation and the resulting soil deformation. Therefore, this paper focuses on the gas accumulation process in which small macroscopic gas bubbles migrate upwards to gradually form large gas bubbles or gas layers, as well as the effect of the formation of gas bubbles on the deformation of the overlying soil layer. The magnesium lithium phyllosilicate (MLPS) transparent soil is selected as the test material, and the morphological parameters, volume, pressure of the gas bubbles formed by gas accumulation in the double-layered soils with upper hard layer and lower soft layer, and the uplift deformation of the overlying soil layer are investigated through gas injection tests by using the image recognition technology. The influences of the strength and height of the overlying soils on the critical state of gas breakthrough are analyzed. The deformation mechanism of the overlying soils under the condition of gas accumulation is explained by applying the thin plate theory. The results reveal the evolution law of gas accumulation in a double-layered soft clay medium, which can guide the establishment of a prediction model for the critical state of accumulated gas breakthrough.

2 Methodology

2.1 Test apparatus

The test apparatus of gas injection into the double-layered transparent soil consists of a visualization system, a gas injection system, and a data acquisition system, as shown in Fig. 1. The test box is a rectangular acrylic plexiglass box without a lid. Two sizes of test boxes are used, i.e. 100 mm×100 mm×150 mm and 200 mm×200 mm×150 mm in length × width×height, to ensure that the gas does not touch the wall during the process of gas accumulation under different test conditions. The four sides of the test box are marked with scales, and the bottom center is provided with a small hole with a diameter of 0.9 mm for the insertion of a stainless-steel needle and gas injection. A high-speed industrial camera (Baumer VCXG-13M) is installed in each of the three orthogonal directions to capture and record in real time the shape of the accumulated gas, with a maximum setting of 90 frames per second. The gas injection rate is controlled by the gas mass flow controller Sevenstar-CS200A with a range of 0−50 cm^3/min and an accuracy of ± 0.35% F.S., where F.S. represents the full-scale value. The gas pressure sensor (MEACON MIK-P3000 monocrystalline silicon) is sampled at 1 kHz to monitor the gas pressure in the delivery line during gas injection in real time, with a range of 0−150 kPa and an accuracy of ±0.075% F.S. All instruments are set up on the level surface of an optical platform.

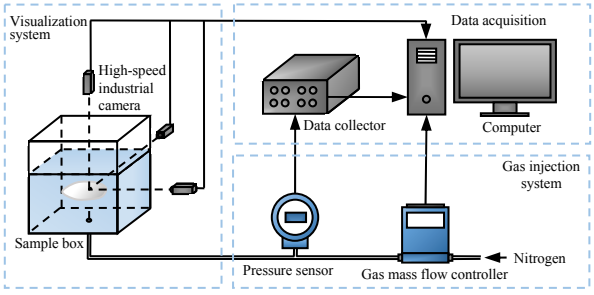

Fig. 1 Schematic diagram of gas injection test equipment

2.2 Test materials and conditions

MLPS transparent soil (commercially known as Laponite RD) is a synthetic lithium alginate with the structure resembling that of natural montmorillonite,

which appears transparent when mixed with water. Measurements of the soil mechanical parameters of MLPS transparent soil by many scholars have shown that it can be used to simulate soft clays with high void ratio, high water content and high compressibility[17−18], and the process and results of the gas injection tests on MLPS transparent soil and natural soils are similar[19]. In this study, MLPS transparent soil with different concentrations was used to simulate the double-layered soils. The concentration of MLPS transparent soil C is defined as

$$C=\frac{m_{\mathrm{l}}}{m_{\mathrm{l}}+m_{\mathrm{w}}}\times 100\% \tag{1}$$

where m_{l} is the mass of MLPS powder; and m_{w} is the mass of deionized water. The stirring device containing the MLPS powder and deionized water was placed in a vacuum tank, and the suspension was poured into the test box after the microbubbles were evacuated under vacuum. The lower layer of transparent soil was kept at a concentration of 3.0% and a height of 6 cm, and the stainless steel needle was inserted to a depth of 1 cm, so that the distance from the gas source to the interface between the upper and lower layers was 5 cm. The lower layer of transparent soil was left to be solidified for 48 h before the upper layer was prepared and added, and the double-layered transparent soil specimen was left to be solidified again for 48 h before the gas injection test. The higher the concentration of the transparent soil, the larger the yield strength. The physico-mechanical parameters of the different concentrations of transparent soil are listed in Table 1. The variables of the test include the concentration and height of the upper layer of transparent soil, with the test conditions listed in Table 2. The test was repeated three times for each test condition. The gas injection rate was 10 cm^3/min. The gas bubbles generated by gas injection at this rate did not form continuous channels that would have an impact on the gas bubbles, leaving the gas bubbles in an environment similar to the natural static growth. All the experiments were conducted at a constant room temperature of 23 °C.

Table 1 Physico-mechanical properties of MLPS transparent soil

Concentration /%	Yield strength /Pa	Poisson's ratio	Modulus of deformation /kPa
3.0	32.8	0.447	—
3.5	49.4	0.436	—
4.0	78.4	0.422	—
4.5	112.7	0.420	63.1
5.0	171.1	0.416	67.5

Note: The data of yield strength and Poisson's ratio were obtained from Zhang et al.[20], while the modulus of deformation was converted from the modulus of compression through consolidation test.

Table 2 Test conditions and parameters

Test condition	Concentration of upper transparent soil /%	Height of upper transparent soil /cm
Nos.1−5	3.5	0.5, 1.0, 1.5, 2.0, 2.5
Nos.6−10	4.0	0.5, 1.0, 1.5, 2.0, 2.5
Nos.11−15	4.5	0.5, 1.0, 1.5, 2.0, 2.5
Nos.16−20	5.0	0.5, 1.0, 1.5, 2.0, 2.5

2.3 Data processing and methods

This study focuses on the changes of morphological parameters, volume, pressure of the gas bubble, and deformation parameters of the upper transparent soil during the evolution of gas accumulation. As shown in Fig. 2, the morphological parameters of the gas bubble and the deformation parameters of the upper transparent soil mainly include the width of the gas bubble W_{g}, the height of the gas bubble h_{g}, the uplift width of the upper transparent soil W_{l}, and the uplift height of the upper transparent soil h_{l}, where h_{g} is the average height of the gas bubbles and is expressed as the ratio of the volume of the gas bubble to the maximum horizontal cross-sectional area.

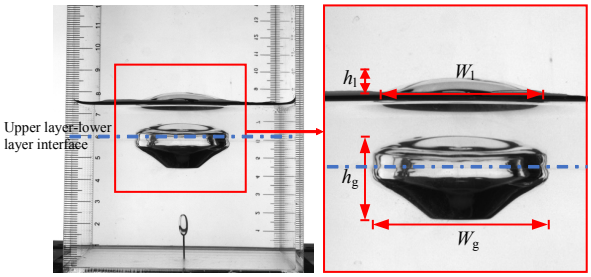

Fig. 2 Schematic diagram of morphological parameters of gas bubble and deformation parameters of upper transparent soil

Matlab was employed to pre-process the gas bubble images captured during the test. The image pre-processing includes five steps, i.e. converting the images to grayscale maps, filtering and denoising, image binarization, hole filling, and edge extraction. The pre-processed images are shown in Fig. 3(a). After the edge extraction of gas bubble was completed, the values of the actual morphological parameters of the gas bubble can be obtained according to the ratio of the image pixels to the real physical length, and the boundary detection error is less than 5%[21]. The gas bubble volume was then obtained by using the modified ellipse-stacking reconstruction method[22], which divides the gas bubble layer by layer into elliptical slices and calculates the long and short semi-axes of each elliptical slice, and then stacks the elliptical slices in turn to generate the three-dimensional (3D) gas bubble morphology to obtain the volume. The reconstructed image of the gas bubble is shown in Fig. 3(b). The uplift width and height of the upper transparent soil were detected by Image-pro Plus software.

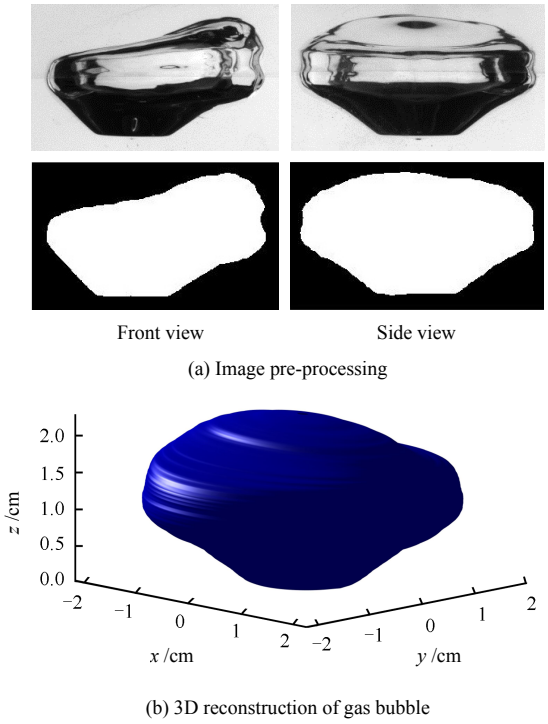

(a) Image pre-processing

(b) 3D reconstruction of gas bubble

Fig. 3 Schematic diagrams of image processing

As the gas bubbles in the transparent soil are in a dynamic process of continuous accumulation and growth, it is difficult to measure the gas bubble pressure directly through the test instrument without damaging the gas bubbles and the surrounding soils. Therefore, in this study, based on the image processing to determine the gas bubble volume, the real-time gas pressure is calculated from the volume through the van der Waals equation, i.e.

$$\left(p+\frac{n^2 m_1}{V^2}\right)(V-nm_2)=nR_0T \tag{2}$$

where V is the volume of the gas bubble, obtained by 3D morphology reconstruction; n is the amount of substance of nitrogen injected, which can be obtained by the injection time t and the injection rate Q. Assuming that the gas was still ideal when entering, we have $n = tQ / V_m$, where V_m is the molar volume of the gas (V_m = 24.3 L/mol). T is the thermodynamic temperature (T= 296 K); m_1 and m_2 are the van der Waals constants for nitrogen (m_1=0.140 8 Pa • m^6 • mol^{-2}, and m_2 = 3.912×10^{-5} m^3 • mol^{-1}); and R_0 is the ideal gas constant (R_0=8.314 J/(mol • K)). The calculated value is the absolute gas pressure of the gas bubble, and subtracting the atmospheric pressure gives the relative gas pressure.

3 Results and discussion

3.1 Evolution of gas accumulation

The morphological evolution of gas accumulation after gas injection in the double-layered MLPS transparent soil is shown in Fig. 4 (test condition No. 10). The single gas bubble formed in the lower layer of 3.0% MLPS transparent soil rises under the action of buoyancy. When it approaches the interface between the upper and lower layers of transparent soil, the gas bubble rises slowly or stops rising due to the higher strength of the upper layer, so that the single gas bubbles gather near the interface between the upper and lower layers, forming an inverted teardrop-shaped gas bubble. With the continuous injection of nitrogen, the upper surface of the gas bubble gradually becomes horizontal and parallel to the interface between the upper and lower layers, and the accumulated gas starts to grow in the horizontal direction, turning into an inverted cone-shaped gas bubble. With the continuous expansion of the upper part of gas bubble, the lower part also undergoes vertical contraction and horizontal development, and the gas bubble gradually develops into the egg tart-like and thick disc shapes. Based on the morphological characteristics of the accumulated gas at each stage in Fig. 4, the morphology of the gas bubble observed evolves over time roughly through four stages: inverted teardrop, inverted cone, egg tart-like and thick disc. The strength and height of the upper layer of transparent soil determine the time t required for gas accumulation and breakthrough and the morphology of the gas bubble when it breaks through the upper layer. As shown in Fig. 5, under the test condition that the concentration C of the upper layer is 4.0% and the height h_t is 0.5 cm, the gas bubble evolves to the inverted teardrop-shape at the first stage before breaking through the upper layer. However, under the test condition that the concentration C of the upper layer is 4.0% and the height h_t is 2.5 cm, the gas bubble evolves through four complete stages to

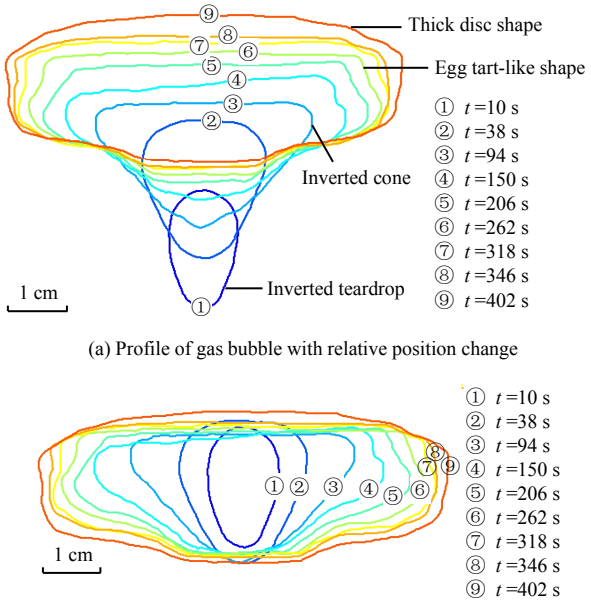

(a) Profile of gas bubble with relative position change

(b) Profile of gas bubble after centroid overlapping

Fig. 4 Evolution of gas form during accumulation in the double-layered MLPS transparent soil

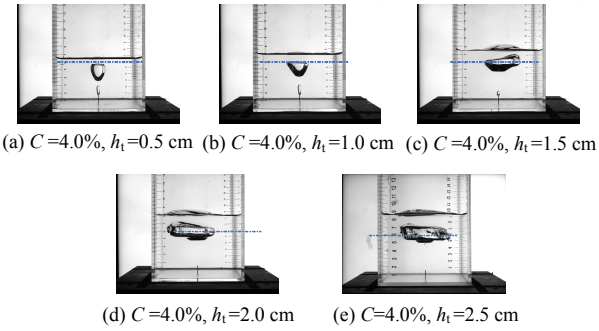

(a) C =4.0%, h_t=0.5 cm (b) C =4.0%, h_t=1.0 cm (c) C =4.0%, h_t=1.5 cm

(d) C =4.0%, h_t=2.0 cm (e) C=4.0%, h_t=2.5 cm

Fig. 5 Forms of accumulated gas before breakthrough under test conditions Nos. 6−10

the thick disc shape before breaking through the upper layer, and the morphology of the bulge on the thick disc-shaped gas bubble before breaking through is similar to that of the shallow gas diapir in the seabed[14]. The higher the strength and the greater the height of the upper layer, the harder the gas bubble breakthrough, and the longer the gas accumulation. As gas accumulation evolves, the upper layer is uplifted upwards and deforms to varying degrees in response to the action of the gas bubble beneath. The longer the gas accumulates and the larger the accumulated volume is, the more apparent the upper layer deforms.

The test condition of the upper soil concentration C equal to 4.0% is still selected as an example herein. Figure 6 shows the morphological parameters, volume and pressure of the gas bubble at different heights of upper transparent soil as a function of injection time. Figure 6(a) shows that the volume of the gas bubble increases linearly with increasing injection time for all test conditions, but there is a clear inflection point at around 100 s. The comparison shows that the growth rate of the gas bubble volume increases by approximately 15% after the inflection point. Combined with the change in gas pressure in Fig. 6(b), the gas pressure peaks at around 100 s for each test condition, which leads to the assumption that during the process of increase in gas pressure, the transparent soil around the gas bubble yields and the plastic zone expands, thus increasing the growth rate of the gas bubble volume. As can be seen from Fig. 6(b), when the thickness of the upper transparent soil is small (h_t = 0.5 and 1.0 cm), the gas breaks through quickly after accumulation, and the gas bubble pressure decreases slowly with time. For the test conditions with a large height of the upper transparent soil (h_t =1.5, 2.0 and 2.5 cm), the gas bubble pressure shows an increasing trend from 0 to 100 s and reaches the peak at around 100 s. After that, the gas bubble pressure drops rapidly and levels off as the growth rate of the gas bubble volume increases. Fig. 6(c) shows that the gas bubble width maintains the same rate of linear growth from 0 to 100 s under all test conditions, while an inflection point occurs at around 100 s. The growth rate of the gas bubble width gradually decreases with increasing gas injection time. Comparing the three test conditions with the heights of 1.5, 2.0 and 2.5 cm indicates that the larger the height of the upper transparent soil is, the slower the growth rate of the gas bubble width decreases, and the greater the final peak is. As shown in Fig. 6(d), the change in the gas bubble height with gas injection time shows a similar trend for all test conditions, i.e. rise–fall–rise. The initial increase in the gas bubble height is due to the coalescence of several gas bubbles one after another to form a long bubble cluster after the start of gas injection. The gas bubble is inverted teardrop-shaped and the duration of this stage is short. Then the gas bubble begins to grow horizontally when encountering the resistance of the upper soil, and contracts vertically under the joint action of resistance of the upper soil and surface tension, reaching the lowest height at around 100 s. After the upper soil yields, the gas bubble starts to accelerate upwards in the vertical direction and the height increases, while the growth of the gas bubble width slows down (also at around 100 s). It is also can be seen from Fig. 7 that the upper soil starts to show obvious uplift deformation at this time. A closer look at the inflection point in Fig. 6(d) where the gas bubble height is located around the injection time of 100 s reveals that the time corresponding to the yielding of the soil varies (88, 98 and 122 s); the greater the height of the upper transparent soil, the longer the time required for yielding. When comparing test conditions with the same upper layer height but different concentrations, a positive correlation is also found between the upper layer concentration and the time required for yielding; the higher the strength, the longer the time required for yielding. For example, when the upper layer height is 2.5 cm, the yielding time is 122, 160 and 200 s for the concentrations of 4.0%, 4.5% and 5.0%, respectively.

The variations of the uplift height and width of upper transparent soil with gas injection time for the upper transparent soil concentration of 4.0% and heights of 1.5, 2.0 and 2.5 cm are shown in Fig. 7. As the upper transparent soil at the heights of 0.5 cm and 1.0 cm did not undergo obvious uplift deformation during the gas injection test, there is no uplift deformation data in the figure. Figure 7(a) shows that the uplift width of upper transparent soil increases linearly with time and then the growth rate decreases, which is similar to that of the gas bubble width, as shown in Fig. 6(c). As shown in Fig. 7(b), the uplift height of upper transparent soil increases approximately linearly with time for each test condition; the greater the upper transparent soil height and the longer the time for gas injection, the lower the growth rate.

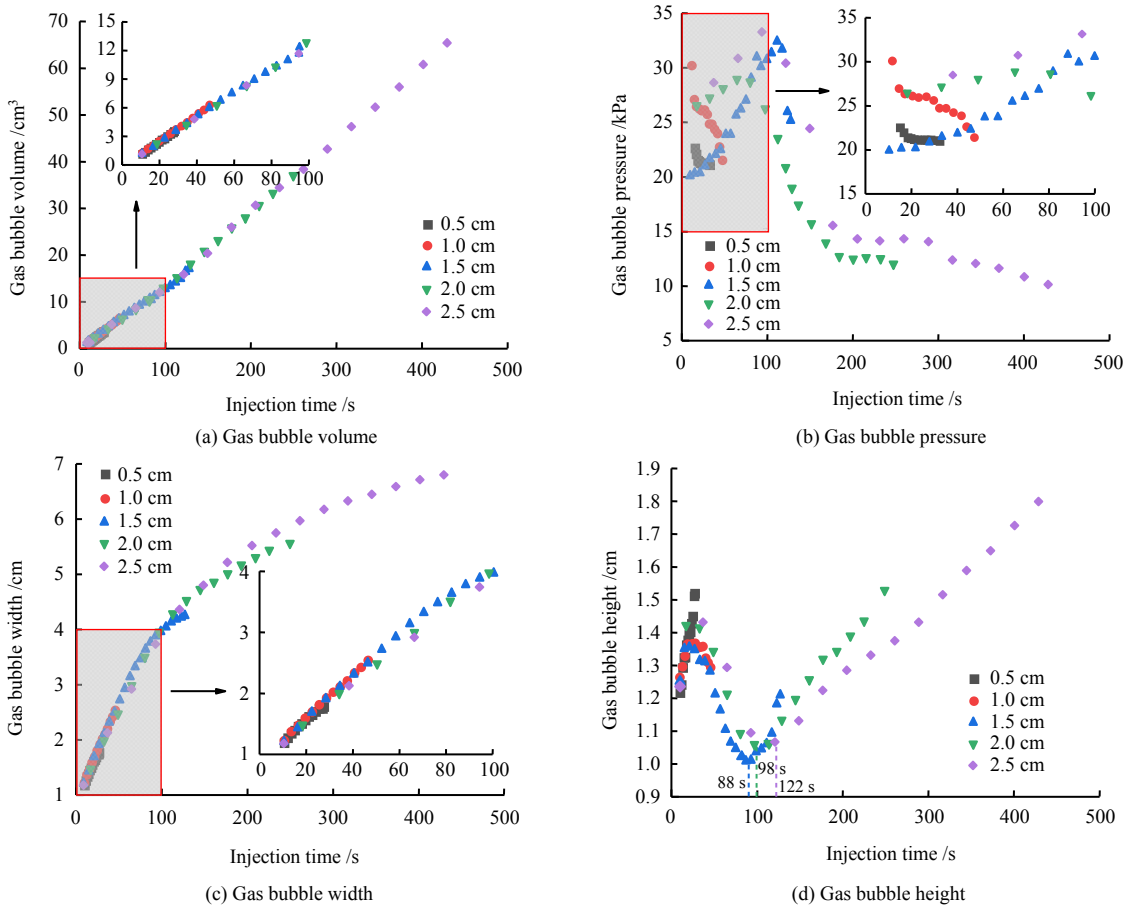

(a) Gas bubble volume (b) Gas bubble pressure

(c) Gas bubble width (d) Gas bubble height

Fig. 6 Changes of gas volume, pressure, width and height during the gas accumulation

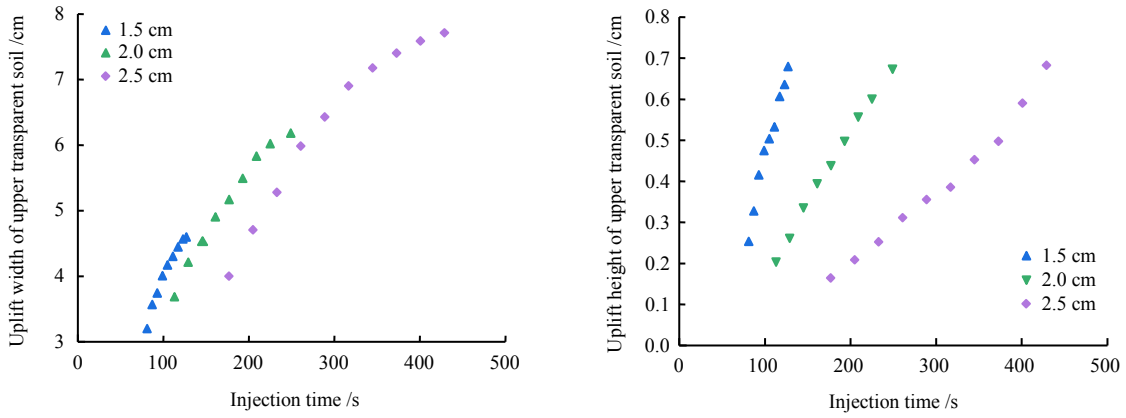

(a) Uplift width of upper transparent soil (b) Uplift height of upper transparent soil

Fig. 7 Changes of uplift width and height of the upper transparent soil during gas accumulation

3.2 Critical state of gas breakthrough

In this study, the last steady state of the gas before escaping from the upper transparent soil to the atmosphere is chosen as the critical state of the accumulated gas breakthrough. To fit the test data, two key influencing factors including yield strength and height of upper transparent soil are normalized. As the lower transparent soil (with 3% concentration) is kept constant in the test, the yield strength and height of lower transparent soil are used as reference values. The ratio of yield strength τ_t / τ_b, and the ratio of height of the upper and lower transparent soils h_t / h_b are used to characterize the yield strength and height of upper transparent soil. It is important to note that the parameters of the lower layer are only adopted for normalization, which will not affect the test results, and other parameters can also be selected for normalization.

The variations in gas bubble width and volume with h_t / h_b for different concentrations of upper transparent soil when the gas breaks through the critical state are shown in Fig. 8. Among them, test condition No. 20 has no valid data, because the gas

bubble touched the test box due to its excessive horizonal size during multiple gas injection tests. As can be seen from Fig. 8(a), the width of gas bubble in the critical state of gas breakthrough does not change significantly with the increase in the height of upper transparent soil when the concentration of upper transparent soil is 3.5%. This is due to the fact that the strength of upper transparent soil at 3.5% concentration is too low, which is smaller than the cracking strength of the gas bubble. Even changing the height of the upper layer cannot effectively prevent the upward escape of the gas. The gas bubble grows to the first stage (inverted teardrop-shape), and then breaks through the upper transparent soil. For the test conditions with the upper transparent soil concentrations of 4.0%, 4.5% and 5.0%, the gas bubble width at the critical state is approximately linear with h_t / h_b; the greater the concentration, the larger the slope of the linearity. By the binary fitting of the gas bubble width W_g with τ_t / τ_b, and h_t / h_b, in the critical state, the relationship between the three parameters can be obtained with the coefficient of determination $R^2 = 0.985$, and the fitting equation is

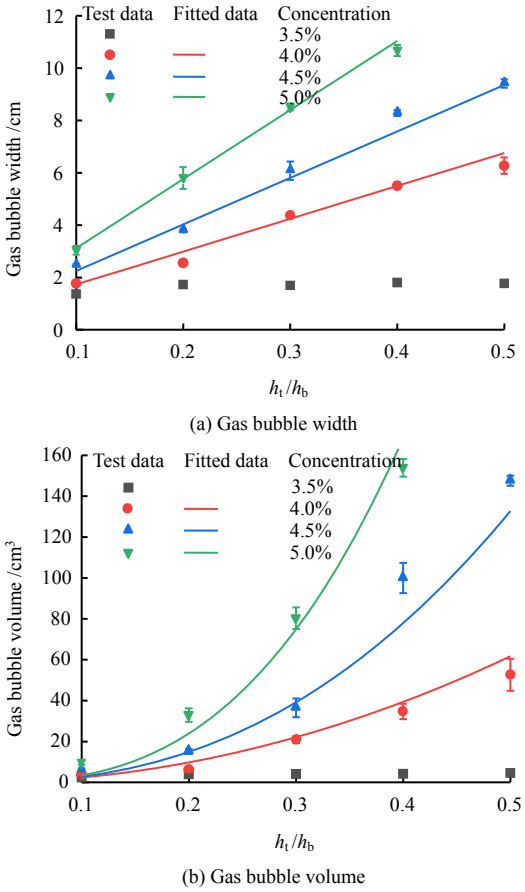

Fig. 8 Variations in gas bubble width and volume at critical state of gas breakthrough under various test conditions

$$W_g = 5.477 \times \left(\frac{\tau_t}{\tau_b}\right)^{0.952} \times \frac{h_t}{h_b} + 0.473 \quad (3)$$

The variations of the gas bubble volume at the critical state of gas breakthrough for each test condition are shown in Fig. 8(b). Similar to the gas bubble width, the gas bubble volume at the critical state does not change significantly with increasing height of the upper transparent soil for the upper transparent soil concentration of 3.5%. For the rest of the upper transparent soil concentrations, the gas bubble volume is a power function of h_t / h_b. The relation between the gas bubble volume V, τ_t / τ_b and h_t / h_b at the critical state of gas breakthrough can be obtained by fitting, with the high coefficient of determination $R^2 = 0.962$, and the equation is written as

$$V = \left(16.90 \times \frac{h_t}{h_b}\right)^{0.890 \times \ln\left(3.860 \times \frac{\tau_t}{\tau_b}\right)} \quad (4)$$

Figure 9 shows the variations of the uplift width and height of upper transparent soil with h_t / h_b at the critical state of gas breakthrough with the upper transparent soil concentrations of 4.0%, 4.5% and 5.0%. At the upper soil concentration of 3.5%, the accumulated gas does not cause significant deformation of the upper soil surface at the critical state of gas breakthrough, thus the deformation data at this concentration are not available in the figure. As can be seen from Fig. 9, the uplift width W_l and uplift height h_l of the upper transparent soil at different upper soil concentrations are linearly related to h_t / h_b, and the relations between W_l, τ_t / τ_b and h_t / h_b can be obtained by fitting as

$$W_l = 7.608 \times \left(\frac{\tau_t}{\tau_b}\right)^{0.579} \times \frac{h_t}{h_b} + 0.315 \times \frac{\tau_t}{\tau_b} \quad (5)$$

$$h_l = 1.012 \times \left(\frac{\tau_t}{\tau_b}\right)^{0.409} \times \frac{h_t}{h_b} + 0.053 \times \frac{\tau_t}{\tau_b} \quad (6)$$

The coefficients of determination R^2 in Eqs. (5) and (6) are 0.984 and 0.934, respectively.

It should be noted that Eqs. (3)–(6) are derived from fitting the data in this test, and similar empirical relationships can be established for natural soils in practical engineering. In addition, the deformation parameters of the upper soils in practical engineering are more intuitive and convenient to obtain, compared to the morphology of the gas accumulated in the soils. Therefore, monitoring the uplift height and extent of soils is of great importance for the establishment of engineering safety early-warning system.

3.3 Calculation of upper transparent soil deformation

As mentioned earlier, it is of great significance to understand the deformation mechanism of the soils under the action of gas accumulation in sediments. Johnson et al.[23] and Barry et al.[24] regarded soft clay sediments and gelatin as linear elastic bodies and

applied the thin plate model to the analysis of seabed dome deformation, arguing that the thin plate theory is also applicable to soft materials. In general, the thin plate theory applies when the ratio of plate thickness h to the minimum size of the plate width (round plate diameter of $2a$) satisfies $1/80< h/(2a) <1/5$; when $h/(2a)$ exceeds 1/5, the medium-to-thick plate theory applies. For the thin plate theory, the ratio of deflection δ to plate thickness h after deformation is not larger than 5, where $\delta/h <1/5$ means small deflection bending of thin plate, and $1/5<\delta/h<5$ means large deflection bending of thin plate.

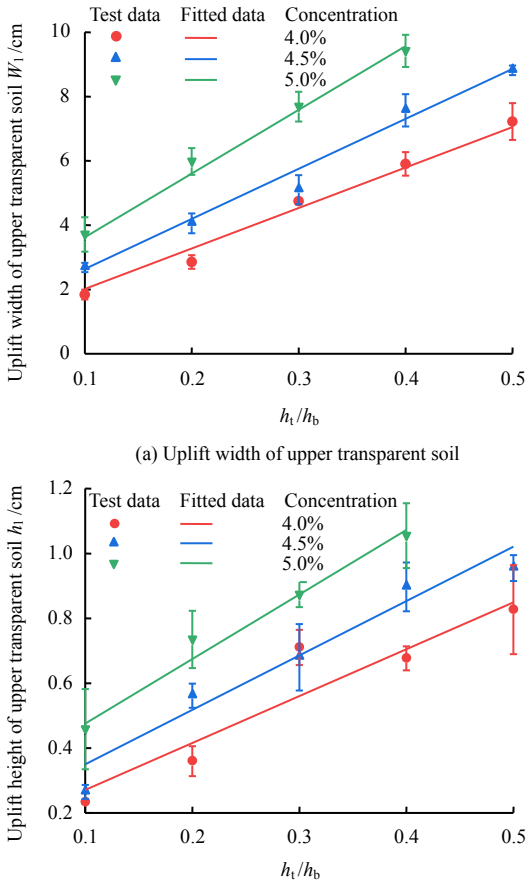

(a) Uplift width of upper transparent soil

(b) Uplift height of upper transparent soil

Fig. 9 Variations in uplift width and height of upper transparent soil at critical state of gas breakthrough under various test conditions

Based on Kirchhoff's hypothesis, the relationship between the deflection δ and the radial distance r in the case of small deflection bending deformation of a thin plate is[25]

$$\delta = \frac{P}{64D}\left(a^2 - r^2\right)^2 \tag{7}$$

where $D = Eh^3/[12(1-\mu^2)]$ is the bending strength; E is the elastic modulus of the material; μ is the Poisson's ratio of the material; and P is the load. The maximum vertical deflection δ_{max} occurs at the center of the plate, i.e. $r = 0$.

When large deflection deformation occurs in a thin plate, it is necessary to consider the mid-plane deformation due to membrane stress in addition to the bending deformation due to bending forces. δ_{max} in the case of large deflection bending deformation of a thin plate satisfies the following equation[25]:

$$P = \frac{64D}{a^3}\left(\frac{\delta_{max}}{a}\right) + \frac{8}{3}\frac{E}{1-\mu}\frac{h}{a}\left(\frac{\delta_{max}}{a}\right)^3 \tag{8}$$

The Reissner medium-to-thick plate theory considers the transverse shear deformation of the plate, and the deflection δ is related to the radial distance r by[26]

$$\delta = \frac{Pa^4}{64D}\left[\left(1-\frac{r^2}{a^2}\right)^2 + \frac{16}{5(1-\mu)}\frac{h^2}{a^2}\left(1-\frac{r^2}{a^2}\right)\right] \tag{9}$$

In this study, the thin plate theory and the medium-to-thick plate theory are used to explain the deformation of the upper transparent soil under the action of gas accumulation. The accumulated gas pressure can be simplified to be a circular uniform load, and the deformed part of the upper transparent soil can be considered as a circular plate of equal thickness with clamped edge. As shown in Fig. 10, the uplift width W_l of the upper soil is the circular plate diameter $2a$; the distance from the upper surface of the gas bubble to the surface of the upper transparent soil is the plate thickness h; the gas bubble pressure p minus the overburden pressure of the circular plate $\rho_l gh$ (ρ_l is the density of the upper transparent soil, and g is the gravity acceleration) is the applied load P; and the uplift height of the upper soil h_l is the maximum vertical deflection δ_{max}.

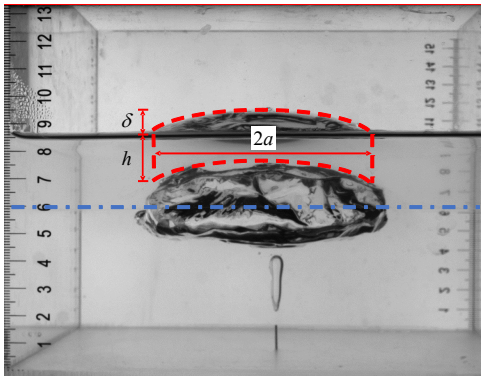

Fig. 10 Schematic diagram of bending deformation of transparent soil simplified as a circular plate of equal thickness under uniform load

Eighteen different transient states are selected for the analysis of the upper transparent soil at the concentration of 4.5% and the heights of 2.0 cm and 2.5 cm, and at the concentration of 5.0% and the heights of 1.5 cm and 2.0 cm, where the upper soil layer is significantly deformed, and the gas bubble is

thick disc-shaped. The δ_c / δ_m values calculated using the thin plate theory and the Reissner medium-to-thick plate theory for each transient state are shown in Fig. 11, where δ_c and δ_m represent the calculated and measured values of the maximum vertical deflection, respectively.

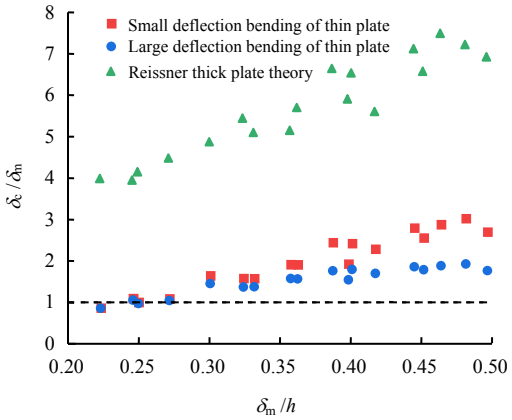

Fig.11 Comparison between thin plate theory and Reissner medium-to-thick plate theory

As shown in Fig. 11, although $h/(2a)$ for each transient state ranges from 0.25 to 0.40, which falls within the interval defined by the Reissner plate theory, δ_c / δ_m values calculated using Reissner plate theory are in the range of 3.8−7.4, which is much greater than that calculated by the thin plate theory. It is indicated that for soft materials such as MLPS transparent soil, the thin plate theory is still more applicable than the Reissner plate theory in this range.

When δ_m / h is between 0.2 and 0.3, the δ_c / δ_m obtained using either the thin plate small deflection bending theory or the large deflection bending theory is between 0.85 and 1.10, which indicates that the small deflection bending theory is still applicable at this time. When δ_m / h exceeds 0.3, the δ_c / δ_m calculated for both small and large deflection bending of thin plate increases as δ_m / h increases, which is consistent with the experimental results of Barry et al.[24]. When δ_m / h is large, $h/(2a)$ affects the accuracy of the thin plate theory; the larger the $h/(2a)$ is, the lower the accuracy is[24]. In this test, $h/(2a)$ is large relative to the definition of a thin plate. In addition, as δ_m / h increases, the gap between δ_c / δ_m of the two theories also widens, which shows that the role of membrane stress increases significantly at this time and the analysis is more accurate using the thin plate large deflection bending theory, which is consistent with Ugural's analysis[25].

Therefore, the deformation of the upper soils due to gas accumulation in double-layered soft sediments can be analyzed effectively by using the thin plate theory. Either the small or large deflection bending theory of thin plate can be selected to reduce the theoretical calculation errors based on the range in which δ_m / h is located. Meanwhile, the thin plate theory can also be used to infer the accumulated gas pressure in the sediments, provided that the maximum vertical deflection parameter at the center of the plate is obtained.

4 Conclusions

In this paper, the evolution of gas accumulation in the double-layered MLPS transparent soil is the main object of study, and the analysis of gas injection tests is carried out with the image recognition technique to investigate the mechanism of gas accumulation and breakthrough in the double-layered soils. The main conclusions are drawn as follows:

(1) The evolution of accumulated gas morphology can be divided into four stages according to the difference in morphological characteristics, i.e. inverted teardrop, inverted cone, egg tart-like and thick disc. The strength and height of the upper soil layer determine the time and morphology of gas bubble at breakthrough.

(2) The volume, pressure, width and height of the gas bubble are interrelated and interact with one another during the process of gas accumulation, and there is an inflection point after the yielding of the soils. Before the inflection point, the volume and width of the gas bubble increase linearly, the gas pressure increases slowly, and the height shows an increase and then a decrease. As the gas pressure increases, the transparent soil yields under the action of the gas pressure, the growth rate of the gas bubble volume increases, and the gas pressure decreases rapidly. The gas bubble accelerates growing upwards in the vertical direction and the height increases significantly. Meanwhile, the growth rate of the gas bubble width in the horizontal direction decreases and tends to level off.

(3) The gas bubble width and volume, as well as the uplift width and height of the upper transparent soil at the critical state of accumulated gas breakthrough can be fitted with the yield strength and the height of upper transparent soil, respectively, which can be used to establish the prediction model of the critical state of accumulated gas breakthrough. The deformation of the upper transparent soil under the action of the accumulated gas can be calculated by the thin plate theory.

In this paper, the evolution of gas accumulation in the double-layered soils is investigated using the transparent soil, and the results are of some reference value in explaining the formation mechanism of gas bubbles in sedimentary layers. Further increase in the thickness or strength of the overlying soil layer will result in the formation of gas bubbles of larger horizontal dimensions. However, due to the nature of the transparent

soil and other factors, the size of the present test equipment cannot be too large, therefore the scale effect of the model test cannot be fully considered, and a strict scale model test needs to be further investigated.

References

[1] CHUVILIN E, SOKOLOVA N, DAVLETSHINA D, et al. Conceptual models of gas accumulation in the shallow permafrost of Northern West Siberia and conditions for explosive gas emissions[J]. Geosciences, 2020, 10(5): 195.

[2] GUO Ai-guo, KONG Ling-wei, SHEN Lin-chong, et al. Study of disaster countermeasures of shallow gas in metro construction[J]. Rock and Soil Mechanics, 2013, 34(3): 769−775.

[3] WANG Y, KONG L, WANG Y, et al. Deformation analysis of shallow gas-bearing ground from controlled gas release in Hangzhou Bay of China[J]. International Journal of Geomechanics, 2018, 18(1): 4017122.1.

[4] CHEN Yun-min, XIE Yan, ZHANG Liang-tong. One-dimensional consolidation model for landfills considering solid-liquid-gas interaction[J]. Chinese Journal of Geotechnical Engineering, 2006, 28(2): 184−190.

[5] YAN Xing-cheng, ZHANG Chong-qian, JI Ming, et al. Concentration of dissolved greenhouse gas and its influence factors in the summer surface water of eutrophic lake[J]. Journal of Lake Sciences, 2018, 30(5): 246−254.

[6] MICHAEL J, JEFFREY P, MICHAEL F, et al. Sediment microstructure and the establishment of gas migration pathways during Bubble growth[J]. Environmental Science & Technology, 2019, 53(21): 12882−12892.

[7] JAIN A K, JUANES R. Preferential mode of gas invasion in sediments: grain-scale mechanistic model of coupled multiphase fluid flow and sediment mechanics[J]. Journal of Geophysical Research: Solid Earth, 2009, 114(B8): B08101:1−B08101:19.

[8] FAURIA K E, REMPEL A W. Gas invasion into water-saturated, unconsolidated porous media: Implications for gas hydrate reservoirs[J]. Earth & Planetary Science Letters, 2011, 312(1−2): 188−193.

[9] SHIN H, SANTAMARINA J C. Open-mode discontinuities in soils[J]. Géotechnique Letters, 2011, 1(4): 95−99.

[10] SUN Hao, GUO Xiu-jun, WU Jing-xin. Progress in analysis and monitoring technology for gas migration in submarine sediments[J/OL]. Progress in Geophysics, 2022, 37(2): 869−881.

[11] LEE S H, CHOUGH S K. Distribution and origin of shallow gas in deep-sea sediments of the Ulleung Basin, East Sea (Sea of Japan)[J]. Geomarine Letters, 2002, 22(4): 204−209.

[12] DIMITROV L, WOODSIDE J. Deep sea pockmark environments in the eastern Mediterranean[J]. Marine Geology, 2003, 195(1): 263−276.

[13] LUAN X W, JIN Y K, OBZHIROV A, et al. Characteristics of shallow gas hydrate in Okhotsk Sea[J]. Science in China (Series D): Earth Sciences, 2008, 51(3): 415−421.

[14] YE Yin-can, CHEN Jun-ren, PAN Guo-fu, et al. Origin, occurrence characteristics and harm to engineering of submarine shallow gas[J]. Donghai Marine Science, 2003(1): 27−36.

[15] LI Ping, DU Jun, LIU Le-jun, et al. Distribution characteristics of shallow gas in offshore seabed of China[J]. The Chinese Journal of Geological Hazard and Control, 2010, 21(1): 69−74.

[16] TAO Ling-fa, PAN Yong-jian, CAI Guo-cheng. The exploration of shallow gas in marine sedimentary soil of the coastal plain[J]. Railway Investigation and Surveying, 2014, 40(4): 47−50.

[17] WALLACE J F, RUTHERFORD C J. Geotechnical properties of Laponite RD[J]. Geotechnical Testing Journal, 2015, 38(5): 574−587.

[18] YE Tian, YI Li-da, HU Meng-xian, et al. Applicability analysis for Laponite RD transparent clay in simulating natural soft clay[J]. Bulletin of Science and Technology, 2019, 35(6): 154−159.

[19] ZHANG Y, CHEN Y, HOU Y, et al. Fracture toughness measurements of soft sediments based on gas injection tests[J]. Marine Georesources & Geotechnology, 2022, 40(7): 1−9.

[20] ZHANG Y, HU M, YE T, et al. An experimental study on the rheological properties of Laponite RD as a transparent soil[J]. Geotechnical Testing Journal, 2019, 43(3): 607−621.

[21] ZHANG Y, HU M, ZHOU Y. An experimental study on bubble growth in Laponite RD as thixotropic yield material[J]. Materials, 2020, 13(13): 2887.

[22] ZHANG Y, QUE X, HU M, et al. 3D reconstruction of a single bubble in transparent media using three orthographic digital images[J]. Applied Sciences, 2020 10(17): 5803.

[23] JOHNSON B D, BOUDREAU B P, GARDINER B S, et al. Mechanical response of sediments to bubble growth[J]. Marine Geology, 2002, 187(3): 347−363.

[24] BARRY M A, BOUDREAU B P, JOHNSON B D. Gas domes in soft cohesive sediments[J]. Geology, 2012, 40(4): 379−382.

[25] UGURAL A C. Stresses in beams, plates, and shells, (Third Edition)[M]. [S. l.]: CRC Press, 2009: 361−363.

[26] HUANG Ke-zhi. Plate and shell mechanics[M]. Beijing: Tsinghua University Press, 1987: 89−104.